Journal of Sound and Vibration 490 (2021) 115723

Contents lists available at ScienceDirect

Journal of Sound and Vibration

journal homepage: www.elsevier.com/locate/jsv

Dynamic acoustic fields for size selective particle separation on centimeter scale

M.H. Kandemir[a,b], M. Beelen[a,b], R.M. Wagterveld[b], D.R. Yntema[b], K.J. Keesman[a,b,*]

[a] Wageningen University & Research, Mathematical and Statistical Methods – Biometris, Droevendaalsesteeg 1, 6708 PB Wageningen, the Netherlands
[b] Wetsus, European Center of Excellence for Sustainable Water Technology, Oostergoweg 9, 8911 MA Leeuwarden, the Netherlands

ARTICLE INFO

Article history:
Received 29 May 2020
Revised 14 September 2020
Accepted 17 September 2020
Available online 19 September 2020

Keywords:
acoustic separation
acoustophoresis
dynamic acoustic fields
selective particle separation

ABSTRACT

Dynamic acoustic fields offer an interesting alternative for acoustic standing-wave fields in acoustic separation applications. This paper reports on an investigation of two methods for generating dynamic acoustic fields and their applicability for selective particle separation. The first method applies a dual-frequency excitation to generate a standing-wave field that in which the pressure nodes travel at constant velocity. The second method uses frequency-ramping, where the velocity of the nodes in the resulting standing-wave field depends on both time and position. Both methods were investigated analytically and with computational models, yielding a dimensionless number that predicts particle behavior without having to solve the differential equations of motion. This dimensionless number can also be used to estimate the acoustic pressure in practical applications. Experiments carried out with polyethylene particles and the two prototypes confirmed the theoretical and numerical predictions. Both methods are suitable for selective particle separation applications.

1. Introduction

Acoustophoresis employs an acoustic radiation force (or sometimes called acoustophoretic radiation force) mostly in a standing-wave field and is one of the methods that can be used to separate particles from suspensions. It is potentially of use for applications in water treatment [1,2]. However, acoustophoresis also offers possibilities for selective separation of particles, as the acoustic radiation force pushes a particle towards either pressure nodes or antinodes, depending on the particle's properties and the drag force it experiences. When a particle has a relative motion with respect to the surrounding liquid, it experiences a drag force. Such relative motion can be in any direction, for example towards a node in an acoustic field [3,4] resulting from an acoustic force, or perpendicular to the acoustic field as a result of flow [5]. The acoustic radiation force scales with the volume of a particle, while the drag force scales with the diameter of the (spherical) particle. Selective particle separation is thus possible based on the size of particles. However, from the theory of acoustic radiation force, it

* Corresponding author: K. J. Keesman, Wageningen University & Research, Mathematical and Statistical Methods – Biometris, Droevendaalsesteeg 1, 6708 PB Wageningen, the Netherlands
E-mail address: karel.keesman@wur.nl (K.J. Keesman).

https://doi.org/10.1016/j.jsv.2020.115723

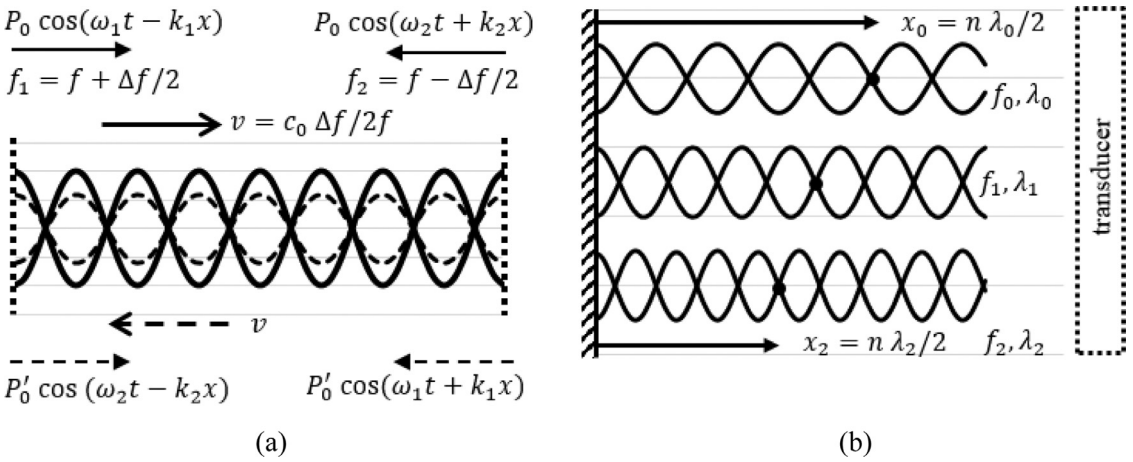

Fig. 1. Two methods for obtaining a pseudo standing-wave field, illustrating the pressure amplitude. (a) Dual-transducer setup, in which two counter-propagating waves create a standing-wave field, which moves at a constant velocity (v, in m s^{-1}) as a result of a small frequency difference (Δf, in s^{-1}) between the two transducers. (b) Transducer-reflector setup, in which the reflector surface is a pressure antinode and use of a frequency sweep (starting at wavelength λ_0) causes the nodes to move.

follows that separation can also take place on the basis of differences in density and compressibility, as acoustic radiation force on a particle depends on these specific particle parameters [2].

Current research on selective particle separation by acoustics mostly focuses on applications in microchannels. The width of such a channel is typically a half-wavelength at the excitation frequency, which means that there is a standing-wave with one pressure node in the middle of the channel. Since the operating frequency is typically in the MHz range, the size of such a channel is in the micrometer range [6-9]. In a dynamic acoustic field, the acoustic force profile is time dependent, in contrast to a stationary standing-wave field [4]. Surface acoustic wave (SAW) applications are examples in which dynamic acoustic fields are used to transport particles [10–21]. Bulk acoustic waves (BAW) also offer possibilities for particle manipulation with dynamic acoustic fields [22]. Whitworth *et al.* [23], for instance, demonstrated a method for transporting particles with two different signals and the use of frequency sweeps. In addition to frequency-ramping, particle manipulation in one or two dimensions is also possible by employing phase differences [24,25]. However, in BAW applications, reflections may significantly disturb the dynamic acoustic field, as addressed by Grinenko *et al.* [26]. Two groups of researchers have numerically investigated particle filtering with frequency-ramped BAW excitation [27,28], and Lipkens *et al.* [29] provided the experimental confirmation. Frequency-ramping is employed in several particle transport applications utilizing BAW [30–32]. Although dynamic BAW fields, in principle, offer the possibility of selective separation on the centimeter scale with multiple nodes, such possibilities have not yet been investigated in detail, to our knowledge.

The objective of the study was therefore to investigate the ability of dynamic BAW fields for selective particle separation on the centimeter scale, and to assess two different methods through numerical simulations and lab experiments. The first method is to generate the field with two different sources operating at slightly different frequencies, effectively resulting in a phase difference that varies linearly with time. The second method is to generate the field with a single source while ramping the excitation frequency, effectively generating a frequency sweep. Theoretical acoustic radiation force expressions were used to estimate particle behavior, a numerical investigation of both methods was carried out using COMSOL Multiphysics. Laboratory experiments with prototypes were conducted to validate the numerical models, and evaluate the performance of these two methods for selective particle separation.

2. Materials and methods

2.1. Dynamic acoustic fields

A standing-wave field results when two counter-propagating waves with the steady (harmonic) waves interact with each other. This interaction can be created by either using two sound sources or using a source and a reflector. With both configurations, it is also possible to generate dynamic BAW fields. In the case of two sound sources with the same amplitude and slightly different frequencies, a pseudo standing-wave field pattern is generated where the nodes move at a constant speed. A dynamic BAW field can also be accomplished by a single sound source operating at a varying frequency, i.e. a frequency sweep. This frequency sweep also leads to a pseudo standing-wave field, but in this case the nodal speed depends on both position and time (see Fig. 1).

2.1.1. Dual-frequency type dynamic fields

Fig. 1a illustrates how two sound sources create a moving standing-wave field. When two acoustic waves with the same amplitude but different frequencies propagate in opposite directions, the total pressure field becomes as follows[1]:

$$P(x,t) = P_0 \cos\left(\omega_2 t + \frac{\omega_2}{c_0}x\right) + P_0 \cos\left(\omega_1 t - \frac{\omega_1}{c_0}x\right) \tag{1}$$

Here, P_0 (Pa) is the common amplitude of the waves, $\omega_1 = 2\pi f_1$ and $\omega_2 = 2\pi f_2$ (rad s^{-1}) are the excitation frequencies, t (s) is time, x (m) is distance from the high frequency source and c_0 (m s^{-1}) is the speed of sound in the host medium. If $\omega_1 = \omega_2$, the sum will be a stationary standing-wave field. When $\omega_1 = \omega_2 + \epsilon$ and $\omega = (\omega_1 + \omega_2)/2$, the field can be written as follows:

$$P(x,t) = 2P_0 \cos\left(\frac{\omega}{c_0}x - \frac{\epsilon}{2}t\right)\cos\left(\frac{\epsilon}{2\ c_0}x - \omega t\right) \tag{2}$$

In such an acoustic field, where $P_D = 2P_0$, the force on a spherical particle is given by Eq. (3)

$$F_x(x,t) = 4\pi k r^3 \left(\frac{P_D^2}{4\rho_0 c_0^2}\right)\Phi(\rho,c)\sin(2kx - \epsilon t) \tag{3}$$

Here, r (m) is the particle radius, ρ_0 (kg m^{-3}) is the density of the medium, ρ is the density of the particle, c is the speed of sound in the particle, $\Phi(\rho, c)$ (-) is the acoustic contrast factor, $k = \omega/c_0$ (m^{-1}) is the wave number and the force field will travel from the higher-frequency source to the lower-frequency source at a constant velocity of $v = \epsilon/2k$ (m s^{-1}). If the frequencies of excitation are given by: $f_1 = f_2 + \Delta f$ and $f = (f_1 + f_2)/2$ (Hz), the velocity of the wave pattern is $v = \frac{\Delta f}{2f} c_0$. A similar field can be created by introducing a phase difference between two sound sources with equal frequencies. Thus, a frequency difference between the sources corresponds to a case in which the phase difference between the sources is shifted linearly and continuously.

In Fig. 1a, the reflected waves (depicted by the dashed line) from the transducer surfaces create a similar but weaker field, which moves in the opposite direction with the same velocity as the applied field. In such a case, with reflections from each transducer surface with a reflection coefficient $R \leq 1$, and neglecting secondary reflections [26], the equation of motion (EOM) of a particle in such a moving field reads as follows:

$$\begin{aligned}&\left(\frac{4}{3}\pi r^3\rho\right)\ddot{x} + (6\pi\mu r)(\dot{x} + u) + 4\pi k r^3\left(\frac{P_D^2}{4\rho_0 c_0^2}\right)\Phi(\rho,c)\sin(2kx - \epsilon t)\\ &+4\pi k r^3\left(\frac{(RP_D)^2}{4\rho_0 c_0^2}\right)\Phi(\rho,c)\sin(2kx + \epsilon t) = 0\end{aligned} \tag{4}$$

Here, u (m s^{-1}) is the constant flow velocity of the liquid from the high-frequency source to the low-frequency source and μ (Pa s) is the viscosity of host medium.

2.1.2. Frequency-sweep type dynamic fields

Fig. 1b illustrates the frequency-ramping method, which employs a sound source and a reflector to obtain the standing-wave field. In this case, the velocity of the nodes depends on position and time and the number of nodes depends on the excitation frequency. A higher frequency wave has more wavelengths per distance, and therefore creates more pressure nodes. When using this method, the modulation type of interest is the frequency sweep. A frequency sweep can be expressed as $f(t) = f_0 + S\,t$ where f_0 is the starting frequency, S is the sweep rate and t is time. The sweep rate S is defined as $S = \Delta f/\Delta t$, where Δf is the sweep frequency and Δt is the sweep period. For practical reasons, the sweep cannot continue infinitely, thus the expression is only valid for a given sweep time and is periodic with sweep period Δt . With the changing frequency, the wavelength also changes, as $\lambda(t) = c/f(t)$. The velocity of any point in the wave pattern is then expressed as (see Appendix A):

$$v(x,t) = -f_0\ /(f_0 + S\,t)^2\ S\,x \tag{5}$$

The distance x is measured from the reflector side. The negative sign of the velocity is due to fact that the reflector is taken as the reference point. Since the frequency changes in time, the wave number $k(t) = \omega(t)/c_0$ also becomes a function of time. Assuming that the maximum pressure amplitude does not vary significantly during the sweep period, the EOM of a particle in such a field therefore becomes

$$\left(\frac{4}{3}\pi r^3\rho\right)\ddot{x} + (6\pi\mu r)(\dot{x} + u) + 4\pi k(t) r^3\left(\frac{P_0^2}{4\rho_0 c_0^2}\right)\Phi(\rho,c)\sin(2k(t)x) = 0 \tag{6}$$

Eqs. (4) and (6) are non-linear, second-order differential equations of motion and have no analytical solution.

[1] For the sake of simplicity in demonstration, only the cosine parts of the waves are considered here.

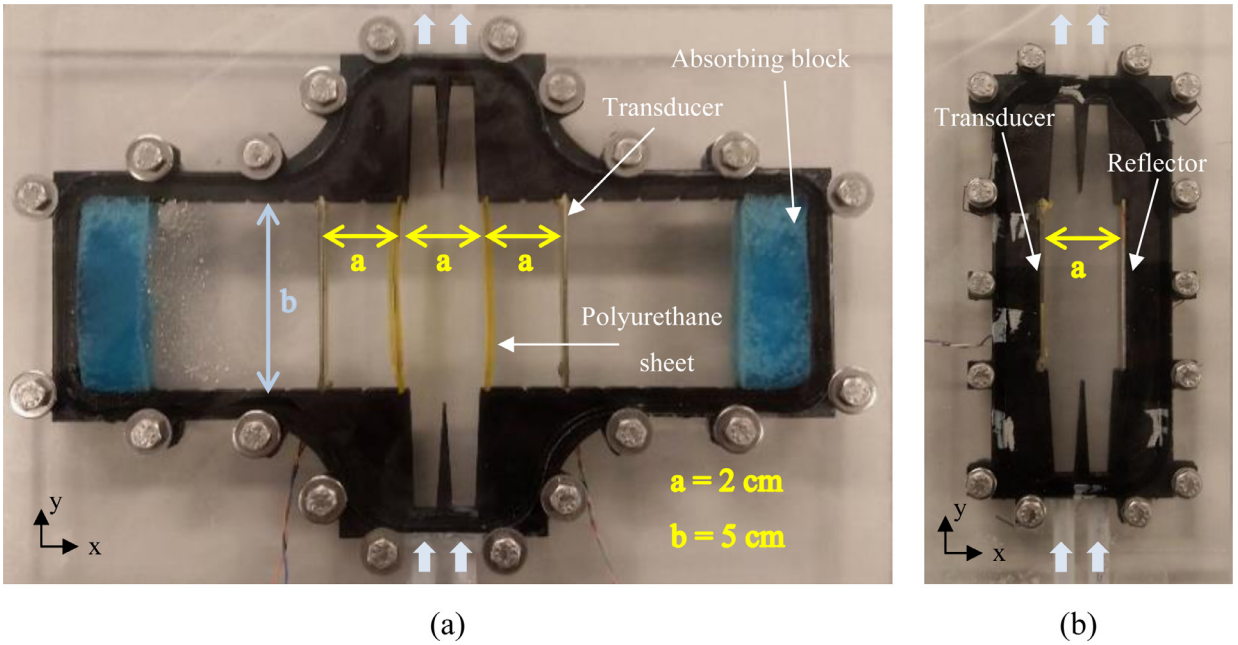

Fig. 2. (color online) Prototypes used in the experiments. Black parts are 3D-printed base structures, with rubber rings used as sealing between base and cover. Each prototype had two inlets and two outlets divided by triangular dividers in the middle of the channel. The width of each separation channel was 20 mm and the depth 10 mm. In prototype (a), used in the dual frequency experiments, the separation channel was bordered by polyurethane sheets with a thickness of 1 mm and the distance between two transducers was 60 mm. The blue parts in (a) are sound-absorbing materials to eliminate back reflections, placed in contact with the end walls and at a distance of 50 mm from each transducer. Prototype (b) was used in the frequency sweep experiments.

2.2. Experimental Setup

The particles used in the experiments were polyethylene particles with a diameter of 70 μm (orange) and 100 μm (blue). The particles had a density of $\rho = 1050$ kg m^{-3} and the speed of sound in the particles was $c = 1720$ m s^{-1}. The used particle mixture contained 1000 cm^3 MilliQ water, with 0.23 g CTAB (hexadecyltrimethylammonium bromide) as surfactant, 0.35 g orange particles and 0.35 g blue particles. Each experimental set-up consisted of a dual-channel signal generator (Keysight Trueform 33512B), a custom-made piezo amplifier, an oscilloscope (Tektronix TDS2024C), two syringe pumps (Aitecs PRO SP-12S) and a separator prototype with piezoelectric transducers. The dual-frequency prototype (Fig. 2a) contained two piezoelectric transducers (Noliac NCE41, dimensions 50 mm $\times$ 10 mm $\times$ 1 mm), two acoustically transparent polyurethane sheets as inner walls and two absorbing blocks (Ecolab kitchen sponge 5 cm $\times$ 1 cm $\times$ 1 cm). The frequency-sweep prototype (Fig. 2b) contained one piezoelectric transducer and a stainless steel reflector plate. Both prototypes, illustrated in Fig. 2, included 3D-printed polylactic acid (PLA) walls and poly(methyl 2-methylpropenoate) (PMMA) covers. The transducers were coated with a thin layer of polyurethane paint to provide electrical insulation. Polyurethane paint is used because it has a similar acoustic impedance as water. In order to verify the effect of the absorbing blocks, admittance measurements are carried out in the prototype. First, the admittance of the transducer placed underwater and away from reflective surfaces is recorded as a function of frequency between 1.8 MHz and 2.5 MHz. When the transducer is placed in the prototype, the admittance was affected due to the natural modes of the water mass between the transducer and the reflective surface, the graph included peaks and valleys related to the natural frequencies of the water mass. When the reflective surfaces are covered with the absorbing block, the peaks and valleys vanished and the admittance graph became similar to that of the transducer alone. Thus, it was concluded that by not reflecting the sound generated by the transducer, the absorbing blocks were preventing the transducer to detect the vibrational modes of the water mass. Admittance measurements for both prototypes are given in Appendix B.

For the dual-frequency experiments, the average frequency was 2.4 MHz and Δf was chosen between 0 Hz and 5 Hz. For the frequency-sweep experiments, the starting frequency f_0 was 2 MHz. The frequency sweep rate, $(f(\Delta t) - f_0)/\Delta t$, is defined by the end frequency ($f(\Delta t)$) and the sweep period (Δt). To enable bubbles (entering from the inlets) to escape the system quickly, the prototypes were on an inclined surface at an angle of 5° with respect to the horizontal plane. Particle motion was recorded by a microscope camera and the particle velocities were calculated by analyzing the movies with ImageJ software [33].

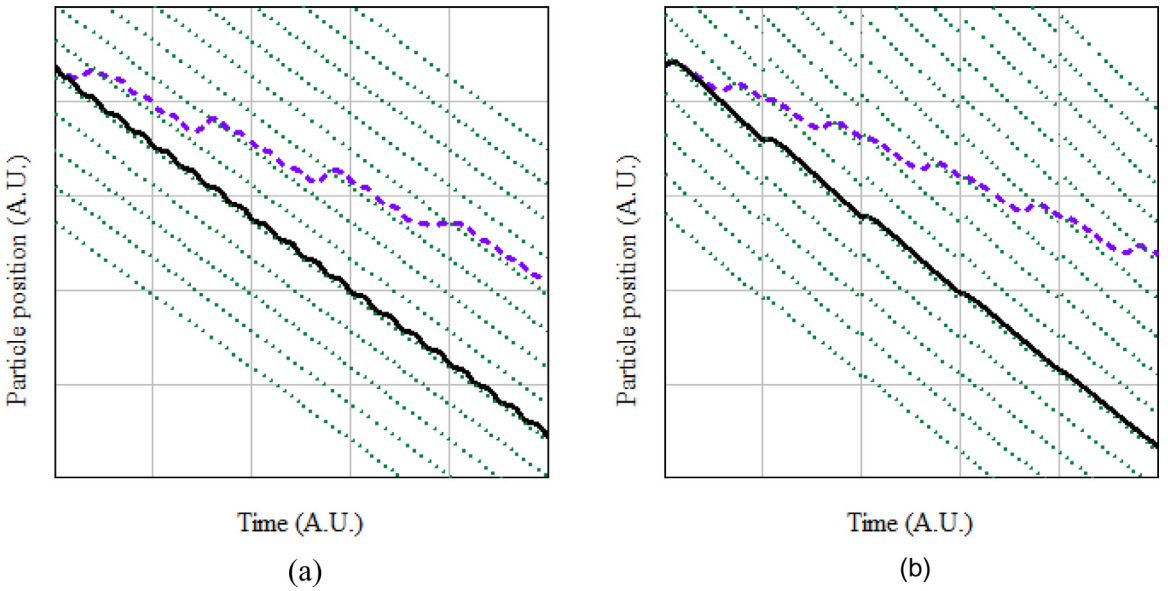

Fig. 3. Typical particle trajectories for particles in dynamic acoustic fields, plotted in arbitrary units for illustration purposes. The captured particle (black solid line) is able to follow the nodal pattern movement (green dotted line) while another particle (purple dashed line) is unable to follow the nodal movement but is still moving downwards. Left panel illustrates a case with a dual-frequency type field and right panel illustrates a frequency-sweep type field. In both cases, the standing wave field is moving downwards. In the dual-frequency case, the reflected field is moving upwards. In the absence of the reflected field a captured particle follows a straight line as the nodal pattern movement.

3. Results and discussion

3.1. Computer simulations

Eqs. (4) and (6) are ordinary differential equations (ODEs) of motion for a particle in a dual-frequency type dynamic field with reflection and frequency-sweep type dynamic field, respectively. In these dynamic fields the nodal pattern is not stationary. Therefore, depending on the particle and excitation properties, a particle may or may not follow the nodal movement. Having the nodal movement in such a way that only the targeted particles are captured is the key for selectivity. For further understanding of the dynamic behavior of the acoustic field and particles within the field numerical simulations were performed.

Fig. 3 illustrates some typical trajectories of captured and non-captured particles in both type of dynamic fields.

Eqs. (4) and (6) can be solved by any software that is capable to solve ODEs. Those equations include the analytical acoustic radiation force expressions on the particle obtained from Gor'kov's method. To check the validity of the analytical force expressions and the equations of motion, the particle trajectories are compared with the trajectories obtained in COMSOL Multiphysics. The comparison is made by including the acoustic radiation force through the use of two different methods in COMSOL. The first method defines the external acoustic radiation force on particles, as given in Eqs. (4) and (6), while the second method numerically calculates the acoustic radiation force on a particle given an acoustic field by using the acoustic field input to the software.

To calculate the acoustic radiation force COMSOL Multiphysics requires the input of the acoustic pressure field and the velocity field. Given that the sound source is much larger than the wavelength, the sound field in our acoustophoresis device is a plane wave field. For small acoustofluidic devices, operating in MHz range and with transducer surface dimensions larger than a millimeter, this is also the case. Hence, the acoustic velocity field can directly be calculated from the pressure field by using the specific acoustic impedance, that is $u(x,t) = \frac{1}{c_0\rho_0}p(x,t)$, where $c_0\rho_0$ is the specific acoustic impedance in the host medium and $u(x,t)$ is the acoustic particle velocity.

Fig. 4 illustrates the case with dual frequency excitation (Fig. 3a) and the resulting particle trajectories calculated in COMSOL by using both methods.

The diameter of the large (captured) particle is $70\,\mu$m and that of the small (non-captured) particle $60\,\mu$m. For both particles, $\rho = 1050$ kg m^{-3}, $c = 1720$ m s^{-1} and $\nu = 0.47125$ (Poisson's ratio). The host medium is water with $\mu = 0.0010093$ Pa s, $\rho_0 = 999.62$ kg m^{-3} and $c_0 = 1481.4$ m s^{-1}. For the dual-frequency type of field excitation parameters are $f = 2.4$ MHz, $\Delta f = 1$ Hz, $u = 0$, $R = 0.8$ and $P_0 = 65$ kPa. The two calculated trajectories of the captured particle, which is thus able to follow the nodal pattern, are (almost) matching and hard to distinguish. Both represent the typical staircase-like movement depicted in Fig. 3a. Trajectories of the small, non-captured particle follow a similar trend, however, they differ especially when the particle is affected more by the next node catching up with the particle.

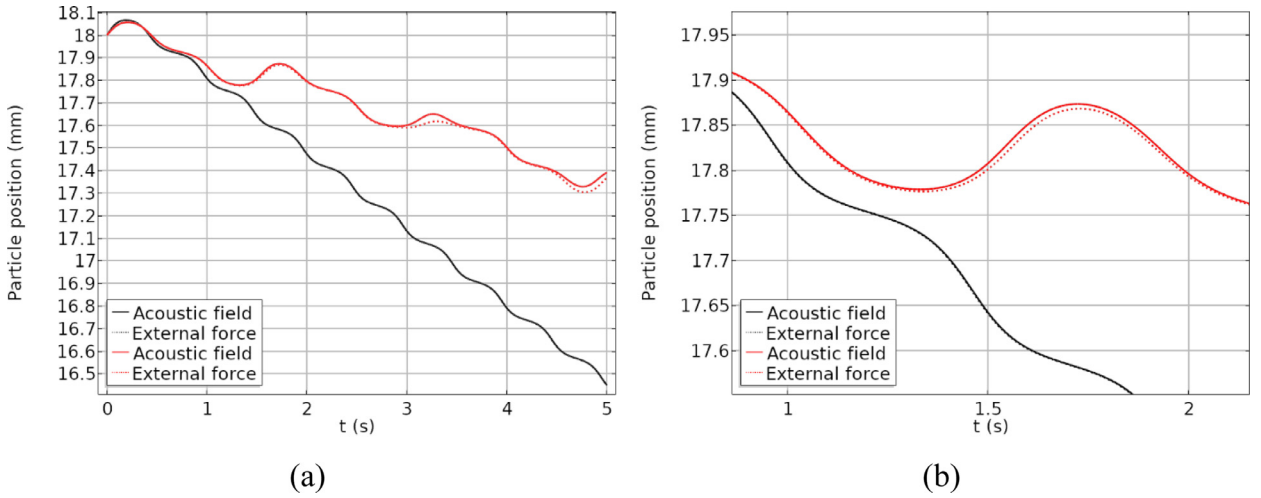

Fig. 4. (a) Particle trajectories calculated by COMSOL. Black lines correspond to the captured particle's ($d = 70$ μm) trajectories and red lines correspond to that of non-captured ($d = 60$ μm) particle. Solid lines are calculated by applying the acoustic radiation force as an external force as in Eq. (4). Dotted lines are calculated by giving the dynamic acoustic fields to COMSOL and the software calculates the acoustic force. (b) Zoomed in view of particle trajectories.

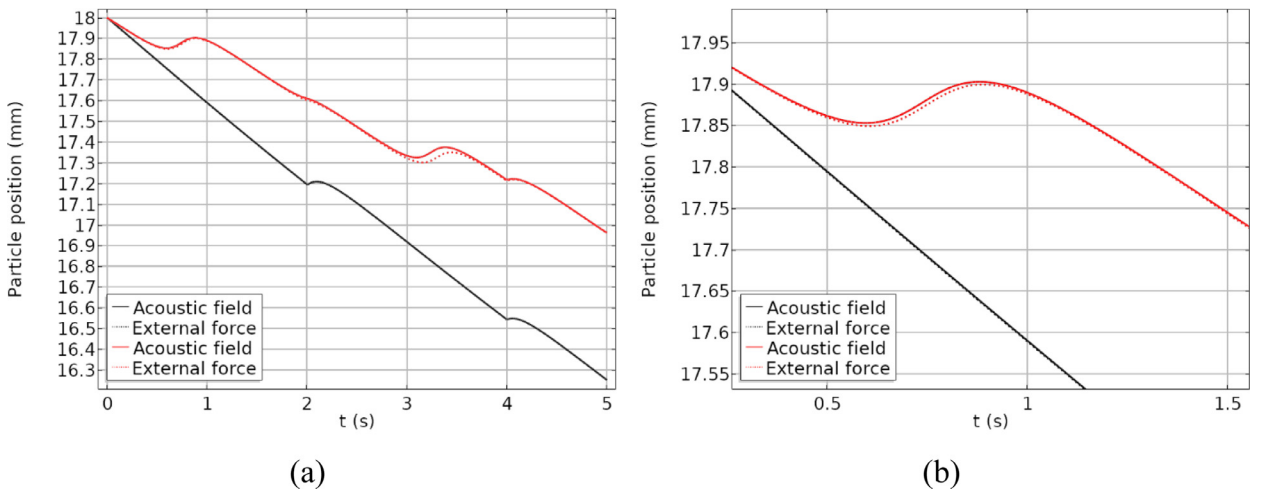

Fig. 5. (a) Particle trajectories calculated by COMSOL. Black lines correspond to the captured particle's ($d = 70$ μm) trajectories and red lines correspond to that of non-captured ($d = 60$ μm) particle. Solid lines are calculated by applying the acoustic radiation force as an external force as in Eq. (6). Dotted lines are calculated by giving the dynamic acoustic fields to COMSOL and the software calculates the acoustic force. (b) Zoomed in view of particle trajectories.

Fig. 5 illustrates the case with frequency-sweep excitation and the resulting particle trajectories calculated by COMSOL.

In Fig. 5, particle properties are the same as the case in Fig. 4. The excitation parameters are $P_0 = 65$ kPa, $f_0 = 2.19$ MHz, $\Delta f = 100$ kHz and $\Delta t = 2$ s. Similar to the dual-frequency case, trajectories of the large, nodal pattern following, particles are matching well. For the small particles, the trajectories follow the same trend while having a deviation especially when the particle is moving upwards as the next node is catching up with the particle.

It should be noted that in both methods, the acoustic field was not calculated by COMSOL. When the force is given as an external force, a generic force node is added to the particle tracing physics tree with the acoustic force expressions in Eqs. (4) and (6) as input. When the acoustic field is input to the "acoustophoretic radiation force" node, the pressure and velocity fields, as shown in Fig. 1, are input for the calculation. Hence, the assumption was that the software does not require a mesh fine enough to resolve the harmonic wave pattern, as the forces acting on the particle were already calculated from functions of time and position. To check this assumption, the same simulations are carried out with the default 'coarse' mesh size in COMSOL and with custom-input mesh size that has maximum element size of $\lambda/12$ at $f = 2.4$ MHz. The acoustic force amplitudes calculated by each method differs less than 0.1%. However, it still makes a difference, especially at moments when the particle is affected by the reflected wave field, as illustrated in Fig. 4.

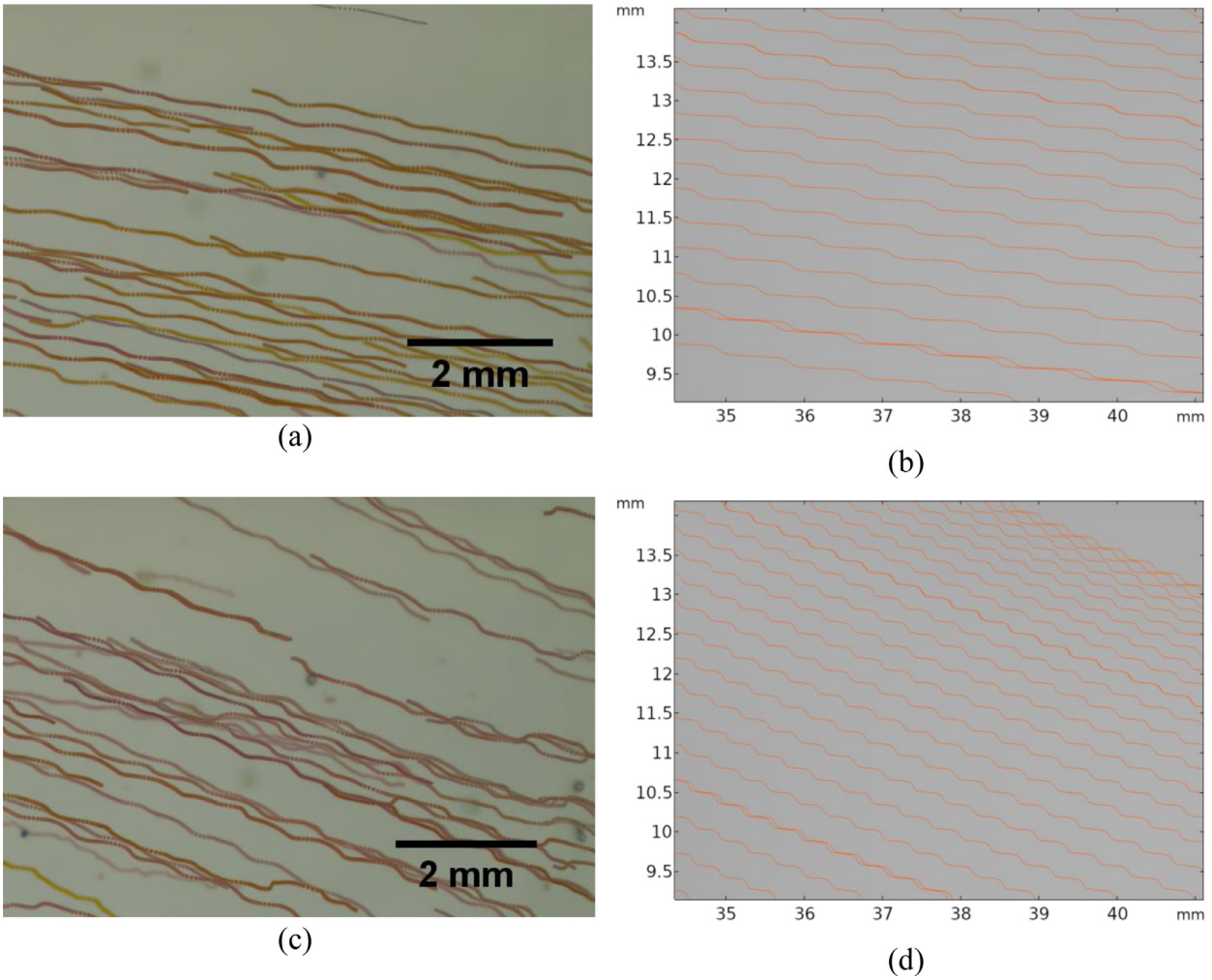

Fig. 6. Experimental and simulated trajectories of the particles in dual-frequency type dynamic field.[2] Flow direction is from left to right and the acoustic field movement is downward. (a) experimental particle trajectories when $\Delta f = 0.4$ Hz. (b) particle trajectories calculated by COMSOL when $\Delta f = 0.4$ Hz. (c) experimental particle trajectories when $\Delta f = 1$ Hz. (d) particle trajectories calculated by COMSOL when $\Delta f = 1$ Hz. In simulations and experiments, $f = 2.4$ MHz. In the experiments, the transducers were excited with $20\,V_{pp}$ while in the simulations $P_0 = 70$ kPa. In the simulations all particles start outside the frame, whereas in the experimental recordings particles do not have a common starting position.

3.2. Experiments

To compare the particle behavior in simulations with those in experiments, a mixture of particles with 70 μm diameter was pumped through the dual-frequency prototype. In one inlet the water-particle mixture was fed and the other inlet was fed with water only, each at a flow rate of 100 $cm^3\ h^{-1}$. Fig. 6 compares the particle trajectories calculated in simulations and the particle trajectories recorded in the experiments, created by overlaying 300 consecutive pictures taken in a span of 10 s.

Fig. 6 confirms the staircase-like particle trajectories, as in Figs 3-4, in case of dual-frequency type excitation and reflection. Fig. 6c includes some particles that do not follow the staircase-like trajectory, which was concluded to be due to the non-uniform size of the particles in the mixture and non-uniformity of the standing wave field. The non-uniformity of the standing wave field is also resulting in some deviations from expected trajectories of particles, without affecting the general trend. The experiments indeed show that if a particle follows the nodal movement, average speed of the particle can be estimated from $v = \frac{\Delta f}{2f} c_0$.

In the dual-frequency type field the nodal pattern and the captured particle velocity is constant and can be estimated by the average frequency and the frequency difference. In the frequency-sweep type field, however, the velocity of the nodal movement is not constant. Taking the origin ($x = 0$) at the reflector surface, Eq. (5) gives the velocity as a function of time and space, which can be used to approximate the average velocity within a sweep period. The average velocity of a captured

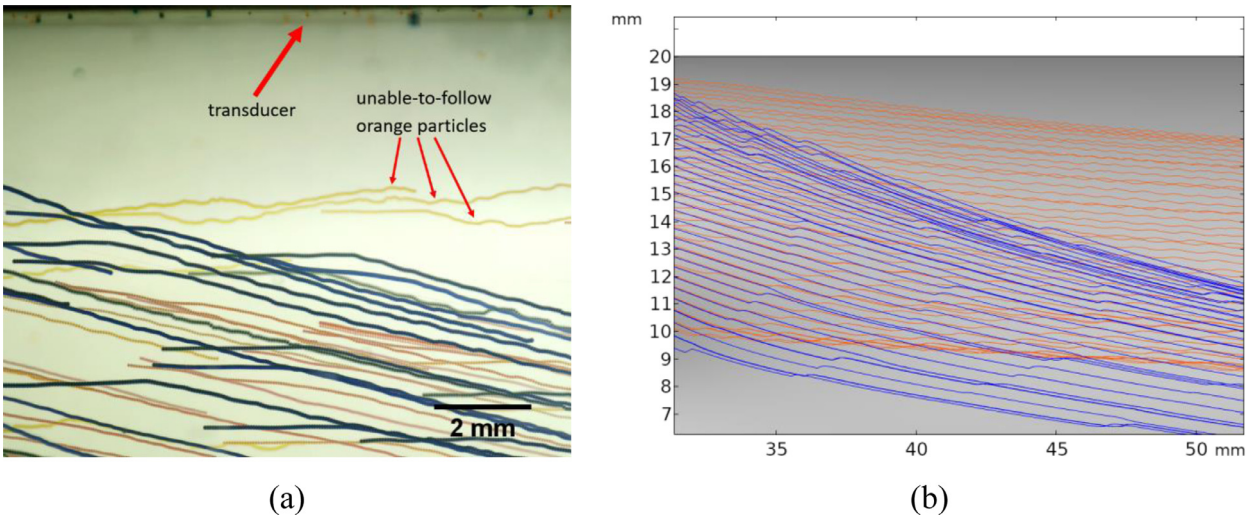

Fig. 7. (a) Experimentally recorded trajectories of two sizes of particles in a frequency-sweep-type dynamic field, obtained by stacking multiple images over time of 10 s, including multiple sweep periods ($\Delta t = 3$ s).[3] Starting frequency was $f_0 = 2.19$ MHz and $f(\Delta t) - f_0 = 300$ kHz. (b) Trajectories of particles from computer simulations with $P_0 = 55$ kPa

particle starting from an initial position x_0, within one sweep period, can be calculated from

$$v_{av} = -\frac{x_0}{\Delta t}\left(1 - \frac{f_0}{f_0 + S\ \Delta t}\right) \tag{7}$$

Fig. 7 compares the particle trajectories resulting from a frequency sweep, calculated in simulations and recorded in experiments. The experimental image is created by overlaying 300 consecutive pictures taken in a span of 10 s.

Fig. 7a displays the experimentally obtained trajectories of particles in a mixture where blue particles having a diameter of 100 μm and orange particles having a diameter of 70 μm. Fig. 7b illustrates trajectories of particles in the same mixture, with $P_0 = 55$ kPa, simulated with COMSOL. The simulation results suggest that even though a particle cannot follow the nodal pattern it will still have a downward motion, as seen in the dual-frequency method. The experimental trajectories do not display a clear separation between the two groups of particles. Besides, the unable-to-follow orange particles are moving in the opposite direction of the nodal pattern.

This last observation can be attributed to a possible aliasing effect that pushes the particles to the closest node, but the closest node is always in the upwards direction. A basic assumption in the simulations is that the pressure amplitude in the standing wave field during the frequency sweep is constant. Depending on the dynamic properties of the transducer, the electromechanical response may differ and result in different peak acoustic pressure. Hence, especially for the non-captured particles the experimental trajectories indicate that there is a force gradient pushing the particles in the opposite direction of the nodal movement.

The velocity expression in Eqs. (5) and (7) suggests that the nodal movement will slow down with increasing time and frequency (Fig. 1b). The nodes further from the reflector ($x = 0$) move faster than the nodes closer to the reflector. For a captured particle, the numerical model and Eq. (7) always yielded lower velocities than those measured in the experiments: This underestimation appears because Eq. (7) predicts the average velocity of a point in the nodal pattern, whereas an actual particle following the nodal pattern has a relative motion with respect to nodal pattern because of the fact that the acoustic force experienced by the particle also changes. Such behavior is explained in detail in Appendix C.

3.3. Conditions for particle capturing

In both types of dynamic fields a captured particle will travel along with the nodal pattern. For the dual-frequency type fields, the nodal pattern has a constant velocity, whereas for the frequency-sweep type fields the nodal velocity can be calculated by Eqs. (5) and (7). Hence, the acoustic radiation force experienced by a particle is proportional to the velocity of the particle in the direction of the nodal movement, therefore balancing the drag force. Fig. 8 illustrates the force experienced by a particle and the corresponding particle velocity in Figs 4 and 5.

The top panels of Fig. 8 correspond to the dual-frequency type dynamic field and the bottom panels correspond to the frequency-sweep type dynamic field. In both cases the force and velocity graphs overlap, indicating that the acoustic force is in balance with the drag force proportional to the velocity, except for Fig. 8c. Fig. 8c confirms, however, by comparing the rate of change of the force (solid line) and velocity (dashed line) for example between $t = 2.5 - 4$ s, that if a particle is following the nodal pattern, it must be moving as fast as or faster than the nodal pattern.

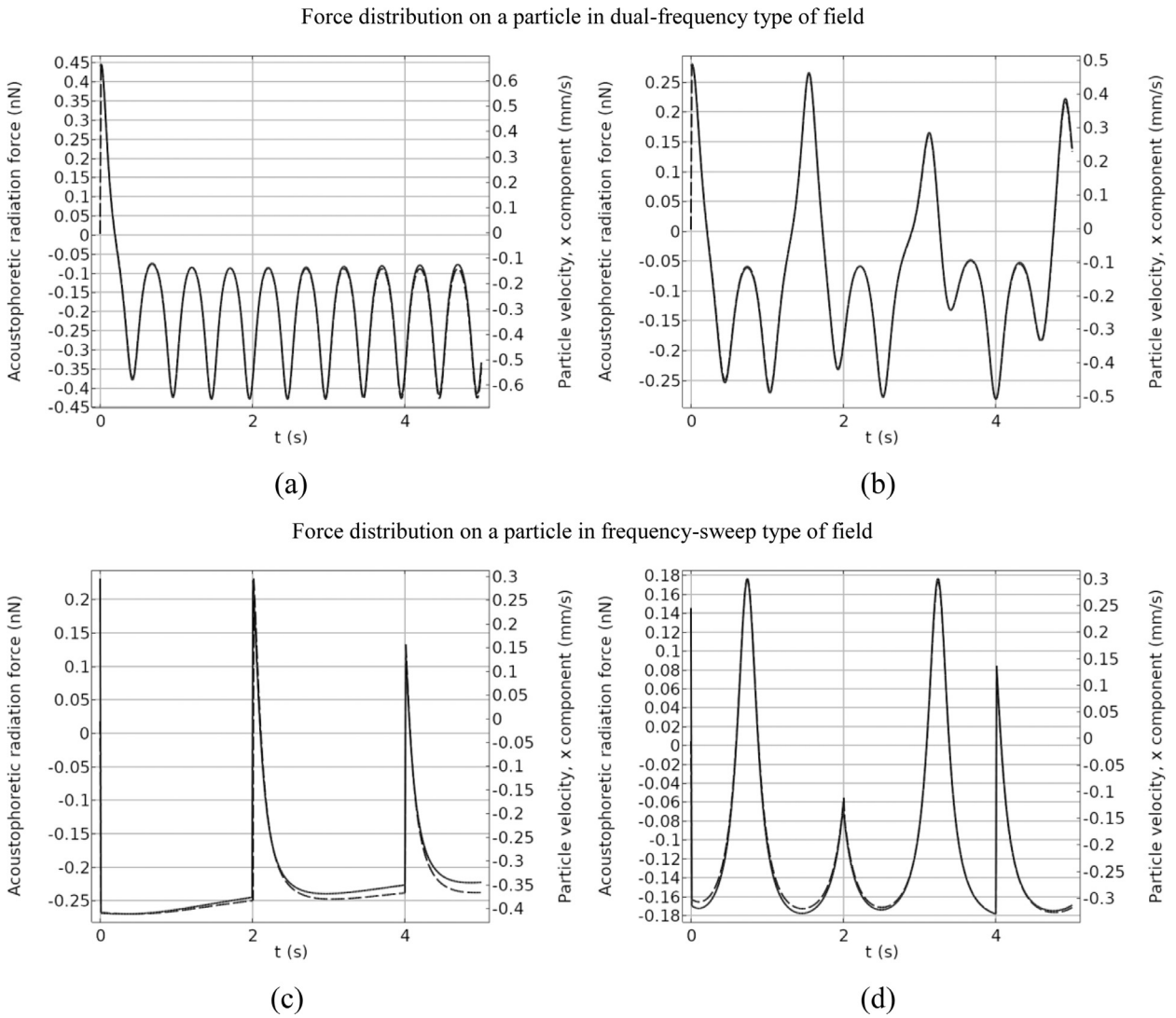

Fig. 8. Time-varying forces (solid lines) and velocities (dashed lines): (a) force and velocity of a captured particle in Fig. 4. (b) force and velocity of a non-captured particle in Fig. 4. (c) force and velocity of a captured particle in Fig. 5. (d) force and velocity of a non-captured particle in Fig. 5.

Under the condition that the particle is following the nodal pattern, the acoustic force must be large enough to overcome the drag force experienced by the particle. Under dual-frequency excitation with $\Delta f \neq 0$, and $u = 0$ and $R = 0$, the following dimensionless number can therefore be defined:

$$K_0 = \frac{F^{max}_{acoustic}}{F^{max}_{drag}} = \frac{4\pi k r^3 \left(\frac{p_0^2}{4\rho_0 c_0^2}\right) \Phi(\rho, c)}{6\pi \mu r \left(\frac{\Delta f}{2f} c_0\right)} \tag{8}$$

This dimensionless number K_0, given in Eq. (8), describes whether the particle is experiencing a large enough acoustic force to follow the nodal pattern. If $K_0 < 1$, the acoustic force on the particle is not large enough to enable it to keep up with the nodal movement ($\frac{\Delta f}{2f} c_0$). $K_0 = 1$ means that the maximum acoustic force equals the drag force on the particle, while $K_0 > 1$ indicates that the particle is able to follow the nodal movement. Fig. 4 showed that, when reflections are present, particles that are able to follow the nodal pattern, thus with $K_0 > 1$, do not move at a constant speed. The counter-propagating dynamic fields interact with each other, and the particles oscillate around the straight-line pattern, forming a staircase-like trajectory. Similar oscillations are present in the paths of the non-captured particles.

In the case of Fig. 4, $K_0 = 1.467$ for the captured particle and $K_0 = 1.078$ for the non-captured particle. Given these K_0 values, both particles should have been able to follow the nodal movement. The presence of reflections, however, disturbs the maximum acoustic force experienced by the particle, although the average force experienced by the particle remains the same, owing to the periodic nature of the two dynamically changing fields. The effect of reflections was explored in

numerical simulations with different excitation parameters (see Appendix D), yielding the following expression for the K number corrected for reflections:

$$K = \frac{K_0}{1 - 3.696 \times 10^{-4}\left(1 - e^{7.582R}\right)} \tag{9}$$

Eq. (9) gives an empirical estimate of K to check whether a particle can follow the nodal movement or not, regardless of whether reflections are present in the system. For the case of Fig. 4, this results in $K = 1.266$ for the captured particle while $K = 0.93$ for the non-captured particle.

For the frequency-sweep type field, Eq. (5) gives the velocity as a function of time and space, which can be used to approximate the average velocity within a sweep period, given in Eq. (7). Hence, Eq. (7) can be inserted into the expression for the K number to estimate if the particle is able to follow the nodal movement. Since the acoustic radiation force also scales with the time-varying wave number, the midpoint at $\frac{1}{2}\Delta t$, should be taken into account. For frequency-sweep type dynamic fields, the dimensionless K number is therefore defined as follows:

$$K = \frac{4\pi k\left(\frac{1}{2}\Delta t\right) r^3 \left(\frac{p_0^2}{4\rho_0 c_0^2}\right) \Phi(\rho, c)}{6\pi \mu r \, \frac{x_0}{\Delta t}\left(1 - \frac{f_0}{f(\Delta t)}\right)} \tag{10}$$

Eq. (10) estimates whether the particle is able to follow the nodal pattern or not, under frequency-sweep conditions. In Fig. 5, $K = 1.07$ for the captured particle and $K = 0.786$ for the non-captured particle. Although the K number estimates the behavior for the first sweep period only (in this case, from 0 to 2 s), it successfully predicts whether the particle is able to follow the field or not.

Numerical simulations suggest that the particle may still be able to move in the direction of the nodal movement and stay between two adjacent nodes if K is larger than 0.9. However, $K \geq 1$ ensures that the particle moves parallel to the nodal movement. If the properties of the particle and of the excitation are known, the K number can also be used to estimate the acoustic pressure in the system. Since $K \geq 1$ implies that the particle is able to follow the nodal movement, it will give a lower bound for the pressure estimate.

Theoretically, the dual-frequency method requires, from Eqs. (1) and (2), that the pressure amplitudes from each source to be equal. The experimental results showed that the captured particles move with average velocity $v = \frac{\Delta f}{2f} c_0$ as predicted by the theory, indicating that the equal pressure amplitude condition is satisfied. If the transducers are identical, equal pressure amplitudes can be assumed and this can be indirectly verified by experiments. Otherwise, the pressure amplitudes need to be calibrated. A common amplitude can be found with the help of, for instance, laser vibrometers. The frequency-sweep method, on the other hand, requires only one source and one reflector, thus a simpler set-up to operate. This simpler set-up creates a nodal movement whose velocity is a function of time and position in the field. Hence, there is no constant nodal velocity among the field. As only one transducer is needed in the system, frequency-sweep methods are expected to consume less energy.

In both cases, the numerical solution of the EOM provides information about the particle path. The analytical force expressions on a spherical particle in a dynamic acoustic field are verified by comparison with the numerical solutions. Expressing the acoustic force as an external force circumvents the necessity of calculating the pressure gradient in COMSOL in order to calculate the acoustic force on a particle. Thus, for simulations where the number of particles are large, the analytical force expressions offer more efficient computation. Whether a particle can follow the nodal movement or not, however, can be estimated without solving the corresponding differential equation (Eq. (4) or (6)). The K number predicts whether the particle can follow the nodal movement.

In summary, computer simulations in COMSOL confirmed the theoretical acoustic radiation force models for both types of dynamic acoustic field. Also, experimental measurements, for both types of dynamic acoustic field, are in line with the particle velocity and trajectory estimates. The dual-frequency type dynamic field creates a constant velocity among the field. The presence of reflections prevents the captured particles to follow a straight line. However, numerical simulations suggest that it is still possible to trap and move particles selectively. This is shown in Fig. 3 and 4, which indicate that it is possible to put a significant distance (in the order of millimeters while particles are in the order of micrometers) between different particles that started at the same location, even when reflections are present in the system. Since reflections disturb the average acoustic force experienced by the particle, it requires a larger pressure for particles to be able to follow the nodal movement when reflections are present. Nevertheless, both methods are suitable for selective particle separation at centimeter scale, the choice of method depends on the expected complexity of the physical system and the predictability of particle behavior.

4. Conclusions

Since dynamic acoustic fields can force different particles into different channels, such fields are particularly useful for selective particle separation as an alternative to stationary standing-wave field applications at centimeter scale. Whether a particle is able to follow the nodal movement in a dynamic acoustic field depends on the properties of the particle and the medium and of the type of excitation, and can thus be predicted beforehand. This study explored two types of dynamic acoustic fields with regard to their applicability toward selective particle separation at centimeter scale.

One type explores dual-frequency dynamic fields, which are generated by two transducers operating at slightly different frequencies, offering constant nodal movement velocities in the separation channel. Although the presence of reflections disturbs the field, these perturbations appear to have little effect on the effectiveness of selective particle separation. Dual-frequency type fields theoretically require equal amplitudes of pressure from both sources.

The other type of investigated dynamic acoustic field is based on frequency-sweep excitation. Such a field is generated with a transducer and a reflector and by ramping the excitation frequency periodically. This is a simpler system with only one transducer and a reflector, but frequency-sweep type dynamic fields do not have a constant nodal velocity in the field. Instead, the nodal velocity depends on position and time. Locations closer to the transducer are more selective with respect to particle separation, as the velocity of the nodal pattern is higher there.

Using the theoretical acoustic radiation force expressions, the dimensionless K number is defined as the ratio between maximum acoustic force and drag force on a particle. The K number, defined for each specific type of dynamic acoustic field, is able to predict whether the particle can follow the nodal movement or not without solving the equations. If $K < 1$ the particle is unable to follow the nodal pattern. The K number can also be used to estimate a lower bound on the acoustic pressure in the system.

Our numerical experiments confirmed the theoretical acoustic radiation force on a spherical particle in a dynamic acoustic field, and lab experiments confirmed the paths and nodal velocities obtained from the numerical models. Both methods for the generation of dynamic acoustic fields, i.e. dual frequency excitation and frequency ramping, are suitable for selective particle separation.

Author contributions

MHK conceived the concept, carried out simulations and wrote the main manuscript. MB carried out experiments and particle velocity calculations MHK, RMW, DRY and KJK reviewed the manuscript.

Declaration of Competing Interest

The author(s) declare no competing interests.

Acknowledgements

This work was performed in the cooperation framework of Wetsus, European Centre of Excellence for Sustainable Water Technology (www.wetsus.nl). Wetsus is co-funded by the Dutch Ministry of Economic Affairs and Ministry of Infrastructure and Environment, the European Union Regional Development Fund, the Province of Fryslãn and the Northern Netherlands Provinces. This work is part of a project that has received funding from the European Union's Horizon 2020 research and innovation program under Marie Skłodowska-Curie grant agreement No 665874. The authors also like to thank the participants of the research theme Dehydration at Wetsus for the fruitful discussions and their financial support.

Supplementary materials

Supplementary material associated with this article can be found, in the online version, at doi:10.1016/j.jsv.2020.115723.

Appendix A. Theory for frequency sweep excitation

If two linear acoustic waves with the same amplitude are traveling in opposite directions, a standing wave pattern is obtained. The simplest way to obtain such a field is by using a transducer as a sound source and a reflector. If the reflector has much higher specific acoustic impedance than the excited medium, the reflector will always be a pressure antinode. Hence, if the frequency of excitation is not constant but changing as a function of time, as in case of frequency sweep excitation while allowing a standing wave to form between the source and the reflector, the standing wave field becomes

$$P(x,t) = P_0 \cos\left(k(t)x\right)\cos(\omega(t)t) \tag{A1}$$

In Eq. (A1), $\omega(t)$ and $k(t)$ are both function of time as the frequency is changed with time. According to Gor'kov[1], the force acting on a spherical particle in x direction can be expressed as

$$F_x = VA_1\frac{\partial}{\partial x}\langle \mathrm{KE}\rangle - VA_2\frac{\partial}{\partial x}\langle \mathrm{PE}\rangle \tag{A3}$$

In Eq. (A3), $V = \frac{4}{3}\pi r^3$ is the particle volume, $A_1 = \frac{3(\rho-\rho_0)}{2\rho+\rho_0}$ and $A_2 = 1 - \frac{\rho_0 c_0^2}{\rho c^2}$ are constants determined by the particle and host medium densities and compressibilities, KE and PE are the temporal averages of the kinetic and potential energy densities of the acoustic field, respectively. Assuming that standing wave field responds fast enough to the change in the excitation frequency, in a plane wave field, the time-averaged potential and kinetic energy densities can be expressed by Eq. (A4) and Eq. (A5), respectively

$$\langle \mathrm{PE}\rangle = E_{ac}\cos^2\left(\frac{\omega}{c_0}x\right) \tag{A4}$$

and

$$\langle \mathrm{KE} \rangle = E_{ac}\left(1 - \cos^2\left(\frac{\omega}{c_0}x\right)\right) \tag{A5}$$

Here, $E_{ac} = \frac{P_0^2}{4\rho_0 c_0^2}$ is the acoustic energy density in the host medium. The acoustic radiation force acting on a spherical particle in x direction is subsequently expressed byEq. (A6)

$$F_x(x,t) = V(A_1 + A_2)E_{ac}\frac{\omega(t)}{c_0}\ \sin\left(\frac{2\omega(t)}{c_0}x\right) \tag{A6}$$

Considering that $k(t) = \omega(t)/c_0$ and replacing the terms for V, A_1 and A_2, the following expression can then be obtained:

$$F_x(x,t) = 4\pi k(t) r^3 \left(\frac{P_D^2}{4\rho_0 c_0^2}\right)\Phi(\rho, c)\sin(2k(t)x) \tag{A7}$$

In Eq. (A7), $\Phi(\rho,c) = \frac{\rho + \frac{2}{3}(\rho - \rho_0)}{2\rho + \rho_0} - \frac{1}{3}\frac{\rho_0 c_0^2}{\rho c^2}$ which is the acoustic contrast factor. In the acoustic contrast factor expression, ρ and ρ_0 denote the particle and host medium densities, respectively. Similarly, c and c_0 denote the speed of sound in the particle and in the host medium, respectively.

In such a standing wave field, velocity of the nodal pattern, and therefore the force pattern is calculated. Taking the reflector as the reference, at the beginning of the sweep period and neglecting the time needed to move from an original position to the closest (anti)nodal line, the distance of a point to the reflector can be expressed as $x(0) = n\ \lambda(0)$. Here, $\lambda(0)$ is the acoustic wavelength in the host medium for $f_0 = f(0)$ and n is a positive number representing the ratio between the wavelength and the initial position. When n is an integer, such positions correspond to the antinodes in the wave field as in Fig. 1b. As time changes, assuming there is a significant acoustic impedance difference between the reflector and the host medium, the reflector will always remain a pressure antinode or a pressure node (Fig. 1b). Therefore, the wave pattern will compress toward the reflector if the frequency is increased. At any time within the sweep period, the distance of the same point in the wave pattern to the reflector is $x(t) = n\ \lambda(t)$ with $\lambda(t) = \frac{c_0}{f(t)}$. Taking $n = x(0)/\lambda(0)$ with $x_0 = x(0)$ and evaluating the time derivative, the velocity of a point in the wave pattern within the sweep period can be expressed as follows:

$$x(t) = \frac{x_0 f_0}{(f_0 + S\ t)} \tag{A8}$$

$$v(x_0,t) = -\frac{f_0}{(f_0 + S\ t)^2}\ S\ x_0 \tag{A9}$$

Here f_0 is the starting frequency, $S$is the sweep rate and t is time. $S := \Delta f/\Delta t$, where Δf is the change of frequency within sweep period Δt. The velocity expression is valid only for the duration of a sweep period and the distance x_0 is measured from the reflector. The velocity expression, Eq. (A9), can be used for any point in the acoustic field at any time within the sweep period. The negative sign is due to the nodes getting closer to the reflector, which is taken as the reference point.

The velocity expression is a function of time and position and makes it possible to calculate the average velocity expressions for different cases. The average velocity for a fixed location x between t_0 and t_1 is calculated as

$$v_{\mathrm{av}}(x,t_0,t_1) = \frac{1}{t_1 - t_0}\int_{t_0}^{t_1} v(x,t)\ dt = -\frac{f_0\ S\ x}{(f_0 + S\ t_0)(f_0 + S\ t_1)} \tag{A10}$$

Similarly, the average velocity in a region between x_0 and x_1 at a given time t is calculated as

$$v_{\mathrm{av}}(t,x_0,x_1) = \frac{1}{x_1 - x_0}\int_{x_0}^{x_1} v(x,t)\ dx = -\frac{1}{2}\frac{f_0\ S\ (x_0 + x_1)}{(f_0 + S\ t)^2} \tag{A11}$$

Finally, the average velocity in a region x_0 and x_1 and in a time interval between t_0 and t_1 is calculated as

$$v_{\mathrm{av}}(x_0,x_1,t_0,t_1) = \frac{1}{x_1 - x_0}\int_{x_0}^{x_1} v_{av}(x,t_0,t_1)\ dx = -\frac{1}{2}\frac{f_0\ S\ (x_0 + x_1)}{(f_0 + S\ t_0)(f_0 + S\ t_1)} \tag{A12}$$

Eqs. (A10)-(A12) can be particularly useful to estimate the average velocity of a group of particles in a region.

For single particles, however, these equations may not be accurate. Assuming that a single particle is able to follow the nodal movement, the velocity of the particle, given Eq. (A11) and $x_1 = x_0 v_{\mathrm{av}}(t_1 - t_0)$, can be expressed as

$$v_{\mathrm{av}}(x_0,t_0.t_1) = \frac{f_0^2\ x_0}{2(t_1 - t_0)}\left(\frac{1}{(f_0 + S\ t_1)^2} - \frac{1}{(f_0 + S\ t_0)^2}\right) \tag{A13}$$

Eq. (A13) requires the knowledge of the initial position and the time. To estimate the average velocity of a particle within one sweep period, since the location of the node will also depend on the time, and using Eq. (A8), the following expression

can be used:

$$v_{\text{av}} = \frac{x - x_0}{\Delta t} = -x_0 \frac{S}{f_0 + S\ \Delta t} \tag{A14}$$

Provided that t_0 and t_1 are within the sweep period and $t_1 > t_0$, the average velocity for a point x between t_0 and t_1 is given by Eq. (A10). The average velocity in a region between x_1 and x_0 at a given time t is given by Eq. (A11). The average velocity in a region $x_0 - x_1$ in a given time interval $t_0 - t_1$ is given by Eq. (A12) but requires the start and end positions as input. Another estimate of the average particle velocity that only requires its initial position to be known is also possible and given by Eq. (A13).

Assuming that the particle is able to follow the nodal movement, all of the four expressions given by Eqs. A10-A13 can be used to approximate the velocity. Such expressions are particularly useful to estimate the average speed of a group of particles in a given time interval and spatial region. The exact average speed of a particle in the first sweep period is given by Eq. (A14). Eq. (A14) was used to estimate the particle velocity and compare it with experimentally derived estimates.

Appendix B. Admittance measurements of the prototypes

In order to check the absorbing blocks are minimizing the reflections, admittance measurements of the prototype were evaluated. Fig. B1 illustrates the admittance measurements for the dual-frequency prototype.

When the absorbing blocks are placed in the prototype, the effect of reflections vanishes as shown in Fig. B1a. In the actual configuration the presence of both transducers causes inevitable reflections, as seen in Fig. B1b. In the operating frequency, both of the transducers have similar admittance.

Fig. B2 illustrates the admittance measurements for the frequency-sweep prototype on the range 1.8 – 2.6 MHz. Sharp peaks indicate high Q factor resonances. The operating range is 2.19 – 2.49 MHz.

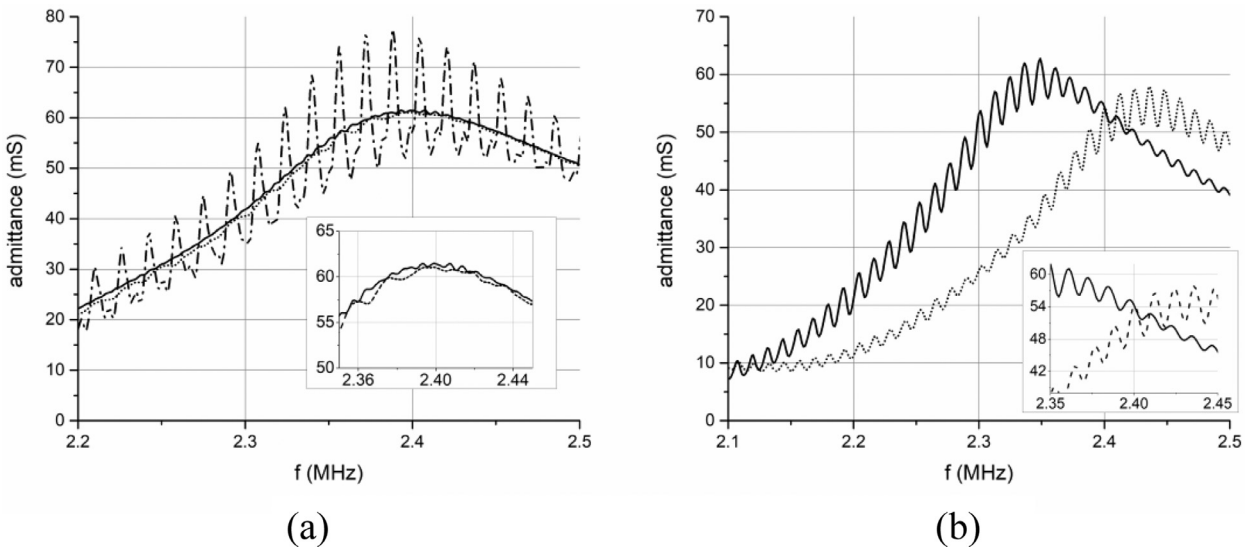

Fig. B1. (a) Admittance of a single transducer. Dash-dot line represents the admittance of the transducer placed in the prototype, solid line represents the admittance of the transducer under water and outside the prototype, dotted line represents the admittance of the transducer when the transducer, absorbing blocks and polyurethane sheets are placed in the prototype. Zoomed window illustrates the latter two cases only. (b) Admittance measurement for two transducers in the prototype including particle solution, absorbing blocks and polyurethane sheets (Fig. 2a). In order to illustrate the effects better zoomed windows were added.

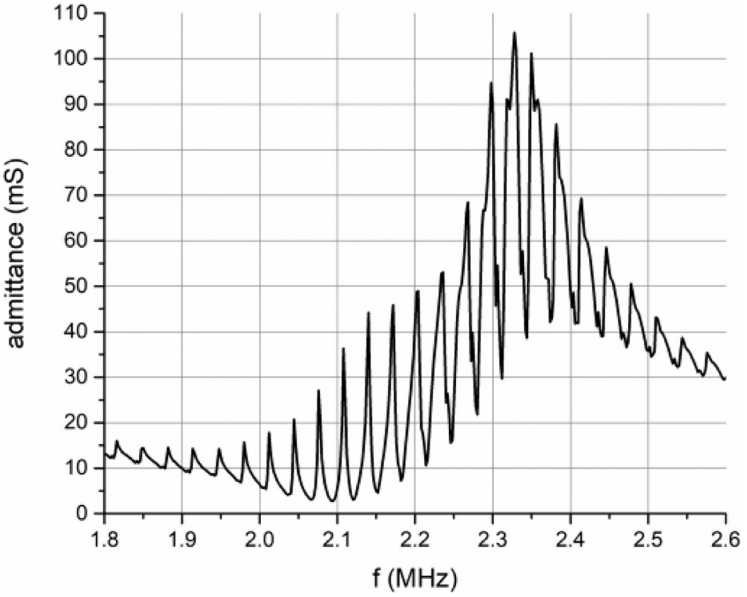

Fig. B2. Admittance of the transducer in the frequency-sweep prototype including particle mixture and reflector (Fig 2b).

Appendix C. Relative motion of a particle in a frequency-sweep type field

If a particle is captured with a frequency-sweep type field, it is expected to follow the nodal pattern. The nodal pattern, however, does not have a constant velocity as indicated in Eq. (5). The velocity of the nodal pattern changes with time and position. Moreover, since the excitation frequency changes, the acoustic energy density in the field also changes. This phenomenon results in a relative motion between a captured particle and the nodal pattern, illustrated in Fig. C1.

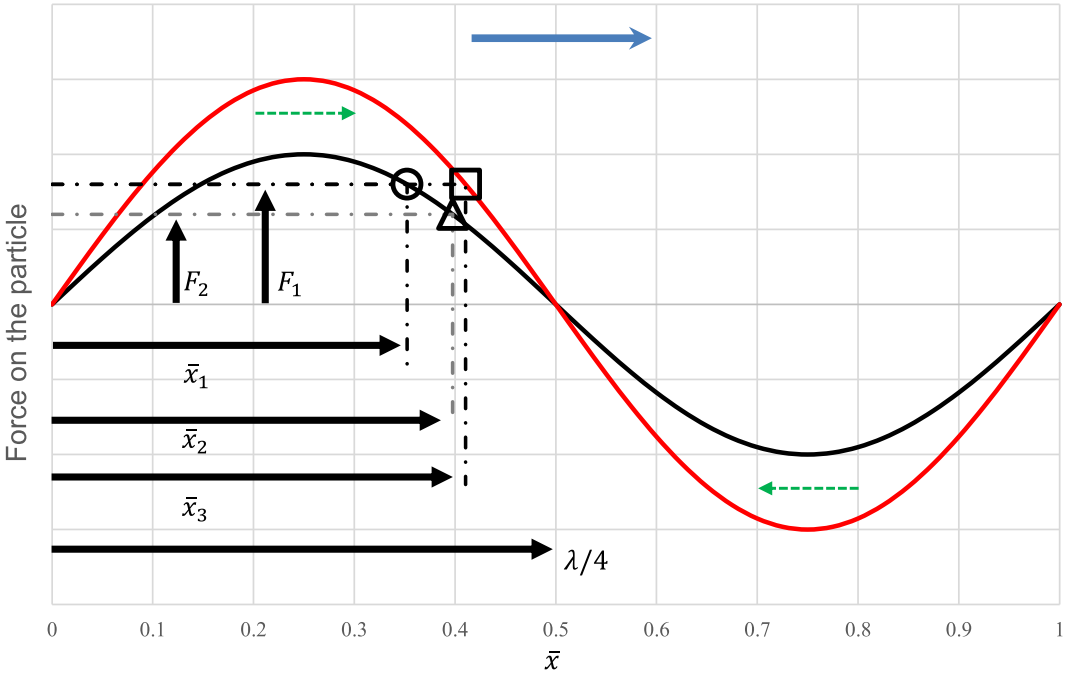

Fig. C1. Equilibrium position of a trapped particle with respect to the moving nodal pattern. Black and red solid lines indicate, in a frequency-sweep-type dynamic field the acoustic radiation force profile acting on a particle as a function of position. Blue arrow indicates the direction of movement of the nodal pattern. Green dashed arrows indicate the direction of acoustic force acting on the particles. The x axis is scaled such that $\bar{x} = x/(\lambda/2)$

Table D1
The threshold K_0 values for different reflection coefficients

R	0	0.1	0.2	0.3	0.4	0.5	0.6	0.7	0.8	0.9
K_0	1	1	1	1.001	1.006	1.02	1.037	1.073	1.157	1.34

In Fig. C1 the nodal pattern is moving in the positive direction. Black line indicates the force field when $f = f_1$ and red line indicates the force field when $f = f_2$, where $f_2 > f_1$. The horizontal axis gives the distance relative to the wavelength, where $\bar{x} = x/(\lambda/2)$.

Consider a particle, initially trapped by the force field given by the black solid line, at $\bar{x}_1$ with force $F = F_1$ in the $\bar{x}$ direction and at time instant $t = t_1$. Assuming the inertial forces are negligible [2], the forces acting on the particle are the drag force and the acoustic radiation force. Given the speed of the nodal pattern, the particle experiences a drag force F_D. In order the particle to be trapped, there must be an acoustic force F_{AC} balancing the drag force, thus $F_{AC} = -F_D$ with magnitude F_1. The line $F = F_1$ intersects the black line in two locations, that is one around $\bar{x} = 0.12$ and another around $\bar{x} = 0.35$. In the absence of an external flow or nodal movement, the acoustic force pattern acts as a restoring force around $\bar{x} = 0.5$, which is the stable trapping location. When a drag force is present, however, the stable trapping location shifts to the intersection at $\bar{x} \approx 0.35$, where $|F_{AC}| = |F_D| = F_1$. Hence, the particle indicated by the circle is initially trapped at location x_1 indicated in Fig. C1. A force equilibrium is also possible around $\bar{x} \approx 0.15$. In this case, however, disturbances at this position result in the particle being trapped away from that location. The latter case is analogous to a particle with positive acoustic contrast factor trapped in the pressure antinode of a stationary standing wave field.

According to Eq. (5), within one sweep period the speed of the nodal pattern slows down with time. Hence, the particle experiences a weaker drag force $|F_D| = F_2$ for $t_2 > t_1$. In the same nodal pattern the particle at t_2, and indicated by the triangle in Fig. C1, has an equilibrium position at x_2, due to similar reasoning with the previous case. The new position x_2 is closer to the pressure node at $\bar{x} = 0.5$ than x_1, therefore the particle goes faster than the nodal pattern while staying in force equilibrium with $|F_{AC}| = |F_D| = F_2$.

In frequency-sweep type fields also the frequency of excitation increases. Eq. (6) suggests that the force amplitude increases with increased frequency. When the frequency is increased from f_1 to f_2, the acoustic radiation force pattern becomes the red solid line in Fig. C1. Keeping the speed of the nodal pattern the same, the particle indicated by the circle has a new equilibrium position, indicated by the square, at x_3 in order to have $|F_{AC}| = |F_D| = F_1$. The new position x_3 is closer to the pressure node at $\bar{x} = 0.5$ than x_1, therefore, again, the particle goes faster than the nodal pattern in order to stay in equilibrium.

The effects mentioned above individually induce a relative motion between the particle and the nodal pattern. In reality, the effects occur simultaneously, hence they together result in a relative motion between the captured particle and the nodal pattern, making the captured particle travel faster than the nodal pattern.

Appendix D. Empirical estimation of the *K* number in the presence of reflections

In the following, the K_0 number is calculated from the ratio of the maximum acoustic force and the maximum drag force on a spherical particle without reflection. The particle will experience the maximum drag force only if it follows the nodal movement. This derivation assumes that there are no reflections in the system, thus there is only the primary dynamic field acting on the particles. When reflections are present, however, a weaker field, due to reflections, still acts on the particles. Numerical simulations were carried out to understand the effect of the reflections on the system.

In the numerical simulations, different random combinations of particle (ρ, c, r) and excitation ($\Delta f, f, P_0$) parameters were evaluated in order to check whether the particle is able to follow the nodal movement or not. The random values are taken from the intervals $500 < \rho < 2000$, $800 < c < 5000$, $2 \times 10^{-6} < r < 100 \times 10^{-6}$ for particle parameters in appropriate SI units, and $0.5 < \Delta f < 10$, $1.5 \times 10^6 < f < 3 \times 10^6$ and $10 \times 10^3 < P_0 < 2 \times 10^6$ for excitation parameters in appropriate SI units. Due to the undiscounted reflections, the condition $K_0 \geq 1$ no longer ensures that the particle is able to follow the nodal movement. The threshold values of K_0, thus under conditions with reflection, for which the particle is able to follow the nodal movement, were recorded from simulations for many combinations of parameters. The threshold K_0 value is a function of reflection coefficient only. Table D1 summarizes the threshold K_0 values for different values of the reflection coefficient.

When the reflection coefficient is larger than 0.9, the threshold values for K_0 become inconsistent, therefore they are excluded from the results. Based on the data obtained in the numerical simulations, the threshold K_0 values can be expressed as a function of the reflection coefficient, that is

$$f(R) = 1 - 3.696 \times 10^{-4}\left(1 - e^{7.582R}\right) \tag{D1}$$

With a correlation coefficient of 0.999 for the non-smoothed simulation data. Fig. (D1) presents the simulated data points and the fitted function.

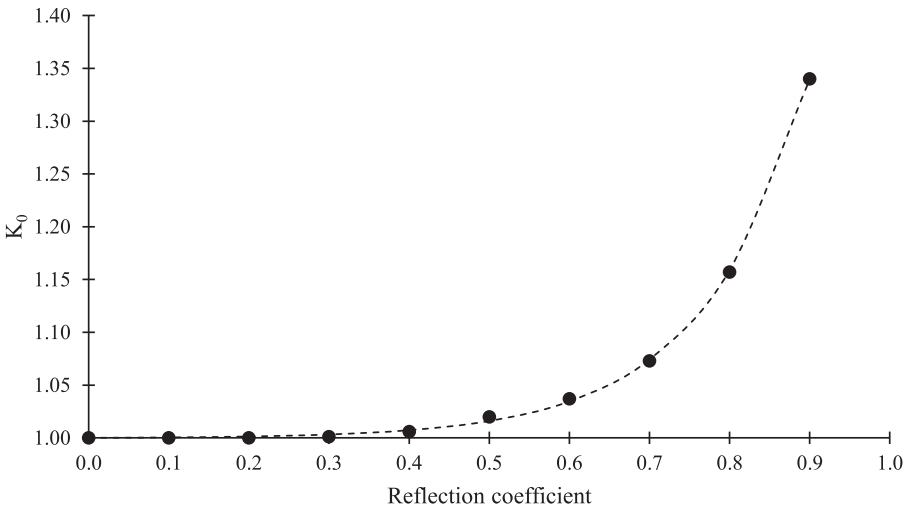

Fig. D1. The threshold K_0 values and the fitted function, $f(R)$. Dots represent the threshold K_0 values for a particle to follow the nodal pattern when reflections are present with given coefficient. The dashed line represents the empirical estimations given by Eq. (D1).

Based on the fitted function using the data from the numerical experiment, the K number as a function of reflection coefficient can be expressed by Eq. (D2)

$$K = \frac{K_0}{1 - 3.696 \times 10^{-4}\left(1 - e^{7.582R}\right)} \tag{D2}$$

with K_0 given by Eq. (4). Numerical simulations confirm that for $R \leq 0.9$, the K number successfully predicts whether the particle is able to follow the nodal movement or not. When $R = 1$, the system shows full reflection, and in such a case a particle simply oscillates around its initial location without following the nodal pattern.

References

[1] L.P. Gor'kov, On the forces acting on a small particle in an acoustical field in an ideal fluid, Sov. Phys. Dokl. 6 (1962) 773–775.
[2] H. Bruus, Acoustofluidics 7: The acoustic radiation force on small particles, Lab Chip 12 (2012) 1014–1021.
[3] H. Bruus, Acoustofluidics 1, Governing equations in microfluidics, Lab Chip 22 (2011) 3742–3751.
[4] H.J. Cappon, Numerical and experimental design of ultrasonic particle filters for water treatment, Ph.D. thesis, Wageningen University, Wageningen, the Netherlands, 2014.
[5] B. Drinkwater, Dynamic-field devices for the ultrasonic manipulation of microparticles, Lab Chip 16 (2016) 2360–2375.
[6] X. Ding, S.-C.S. Lin, M.I. Lapsley, S. Li, X. Guo, C.Y. Chan, I.K. Chiang, L. Wang, J.P. McCoy, T.J. Huang, Standing surface acoustic wave (SSAW) based multichannel cell sorting, Lab Chip 12 (2012) 4228–4231.
[7] S. Kapishnikov, V. Kantsler, V. Steinberg, Continuous particle size separation and size sorting using ultrasound in a microchannel, J. Stat. Mech. Theory Exp. 2006 (2006) P01012–P01012.
[8] F. Petersson, L. Aberg, A.M. Swärd-Nilsson, T. Laurell, Free flow acoustophoresis: microfluidic-based mode of particle and cell separation, Anal Chem 79 (2007) 5117–5123.
[9] T. Laurell, F. Petersson, A. Nilsson, Chip integrated strategies for acoustic separation and manipulation of cells and particles, Chem. Soc. Rev. 36 (2007) 492–506.
[10] G. Simon, J. Marques-Hueso, M.P. Desmulliez, A.L. Bernassau, D. Roolvink, G. Burns, P.A.G. Cormack, M.A.B. Andrade, J. Reboud, J.M. Cooper, M.O. Riehle, Reconfigurable particle separation by dynamic acoustic fields in microfluidic devices, 24th International Conference on Sound and Vibration, London, United Kingdom, 2017.
[11] F. Guo, Z. Mao, Y. Chen, Z. Xie, J.P. Lata, P. Li, L. Ren, J. Liu, Three-dimensional manipulation of single cells using surface acoustic waves, Proc. Natl. Acad. Sci. U. S. A. 113 (2015) 1522–1527.
[12] S.B.Q. Tran, P. Marmottant, P. Thibault, Fast acoustic tweezers for the two-dimensional manipulation of individual particles in microfluidic channels, Appl. Phys. Lett. (2012) 101.
[13] N.D. Orloff, J.R. Dennis, M. Cecchini, E. Schonbrun, E. Rocas, N.D. Orloff, J.R. Dennis, M. Cecchini, E. Schonbrun, E. Rocas, Y. Wang, D. Novotny, R.W. Simmonds, J. Moreland, I. Takeuchi, J.C. Booth, Manipulating particle trajectories with phase-control in surface acoustic wave microfluidics, Biomicrofluidics (2011) 5.
[14] L. Meng, F. Cai, Z. Zhang, L. Niu, Q. Jin, F. Yan, J. Wu, Z. Wang, H. Zheng, Transportation of single cell and microbubbles by phase-shift introduced to standing leaky surface acoustic waves, Biomicrofluidics (2011) 5.
[15] C.D. Wood, J.E. Cunningham, R.O. Rorke, C. Wälti, E.H. Linfield, A.G. Davies, S.D. Evans, C.D. Wood, J.E. Cunningham, R.O. Rorke, C. Wälti, E.H. Linfield, Formation and manipulation of two-dimensional arrays of micron-scale particles in microfluidic systems by surface acoustic waves, Appl. Phys. Lett. (2009) 94.
[16] G. Simon, M.A.B. Andrade, J. Reboud, J. Marques-hueso, M.P.Y. Desmulliez, M. Jonathan, M.O. Riehle, A.L. Bernassau, G. Simon, M.A.B. Andrade, J. Reboud, J. Marques-hueso, M.P.Y. Desmulliez, J.M. Cooper, M.O. Riehle, A.L. Bernassau, Particle separation by phase modulated surface acoustic waves, Biomicrofluidics (2017) 11.
[17] G. Simon, Y. Pailhas, M.A.B. Andrade, J. Reboud, J. Marques-hueso, M.P.Y. Desmulliez, J.M. Cooper, M.O. Riehle, A.L. Bernassau, G. Simon, Y. Pailhas, M.A.B. Andrade, J. Reboud, J. Marques-hueso, M.P.Y. Desmulliez, J.M. Cooper, M.O. Riehle, A.L. Bernassau, Particle separation in surface acoustic wave microfluidic devices using reprogrammable, pseudo-standing waves, Appl. Phys. Lett. (2018) 113.
[18] X. Ding, S.S. Lin, B. Kiraly, H. Yue, S. Li, I. Chiang, J. Shi, On-chip manipulation of single microparticles, cells, and organisms using surface acoustic waves, Proc. Natl. Acad. Sci. U. S. A. 109 (2012) 11105–11109.

[19] D.J. Collins, R.O. Rorke, C. Devendran, Z. Ma, J. Han, A. Neild, Y. Ai, Self-Aligned Acoustofluidic Particle Focusing and Patterning in Microfluidic Channels from Channel-Based Acoustic Waveguides, Phys. Rev. Lett. (2018) 120.
[20] J. Lee, C. Rhyou, B. Kang, H. Lee, Continuously phase-modulated standing surface acoustic waves for separation of particles and cells in microfluidic channels containing multiple pressure nodes, J. Phys. D. Appl. Phys. (2017) 50.
[21] C. Rhyou, S. Park, H. Lee, Optimal rate for continuous phase modulation in standing surface acoustic waves, J. Mech. Sci. Technol. 33 (2019) 3819–3829.
[22] G.D. Skotis, D.R.S. Cumming, J.N. Roberrty, M.O. Riehle, A.L. Bernassau, Dynamic acoustic field activated cell separation (DAFACS), Lab Chip 15 (2015) 802–810.
[23] G. Whitworth, M.A. Grundy, W.T. Coakley, Transport and harvesting of suspended particles using modulated ultrasound, Ultrasonics 29 (6) (1991) 439–444.
[24] C.R.P. Courtney, C.-K. Ong, B.W. Drinkwater, P.D. Wilcox, C. Demore, S. Cochran, P. Glynne-Jones, M. Hill, Manipulation of microparticles using phase–controllable ultrasonic standing waves., J. Acoust. Soc. Am. 128 (2010) EL195–EL199.
[25] C.R.P. Courtney, C.-K. Ong, B.W. Drinkwater, a.L. Bernassau, P.D. Wilcox, D.R.S. Cumming, Manipulation of particles in two dimensions using phase controllable ultrasonic standing waves, Proc. R. Soc. A Math. Phys. Eng. Sci. 468 (2011) 337–360.
[26] A. Grinenko, C.K. Ong, C.R.P. Courtney, P.D. Wilcox, B.W. Drinkwater, A. Grinenko, C.K. Ong, C.R.P. Courtney, P.D. Wilcox, B.W. Drinkwater, Efficient counter-propagating wave acoustic micro-particle manipulation, Appl. Phys. Lett. 101 (2012) 9–12.
[27] B. Lipkens, M. Costolo, E. Rietman, The effect of frequency sweeping and fluid flow on particle trajectories in ultrasonic standing waves, IEEE Sens. J. 8 (2008) 667–677.
[28] F.J. Trujillo, S. Eberhardt, D. Möller, J. Dual, K. Knoerzer, Multiphysics modelling of the separation of suspended particles via frequency ramping of ultrasonic standing waves, Ultrason. Sonochem. 20 (2013) 655–666.
[29] B. Lipkens, J. Dionne, A. Trask, B. Szczur, A. Stevensa, E. Rietmana, Separation of micron-sized particles in macro-scale cavities by ultrasonic standing waves, Phys. Procedia. 3 (2010) 263–268.
[30] O. Manneberg, B. Vanherberghen, B. Onfelt, M. Wiklund, Flow-free transport of cells in microchannels by frequency-modulated ultrasound, Lab Chip 9 (2009) 833–837.
[31] A. Haake, A. Neild, G. Radziwill, J. Dual, Positioning, Displacement , and Localization of Cells Using Ultrasonic Forces, Biotechnol. Bioeng 92 (2005) 8–14.
[32] A. Haake, J. Dual, Contactless micromanipulation of small particles by an ultrasound field excited by a vibrating body, J. Acoust. Soc. Am. (2015) 117.
[33] J. Schindelin, I. Arganda-carreras, E. Frise, V. Kaynig, M. Longair, T. Pietzsch, S. Preibisch, C. Rueden, S. Saalfeld, B. Schmid, J. Tinevez, D.J. White, V. Hartenstein, K. Eliceiri, P. Tomancak, A. Cardona, Fiji : an open-source platform for biological-image analysis, Nat. Methods 9 (2012) 676–682.